

Skill of seasonal rainfall and temperature forecasts for East Africa

Article

Accepted Version

Young, H. R. ORCID: <https://orcid.org/0000-0002-7997-9471>
and Klingaman, N. P. ORCID: <https://orcid.org/0000-0002-2927-9303> (2020) Skill of seasonal rainfall and temperature forecasts for East Africa. *Weather and Forecasting*, 35 (5). pp. 1783-1800. ISSN 0882-8156 doi: <https://doi.org/10.1175/WAF-D-19-0061.1> Available at <http://centaur.reading.ac.uk/91641/>

It is advisable to refer to the publisher's version if you intend to cite from the work. See [Guidance on citing](#).

Published version at: <https://journals.ametsoc.org/waf/article/doi/10.1175/WAF-D-19-0061.1/353353/Skill-of-seasonal-rainfall-and-temperature>

To link to this article DOI: <http://dx.doi.org/10.1175/WAF-D-19-0061.1>

Publisher: American Meteorological Society

All outputs in CentAUR are protected by Intellectual Property Rights law, including copyright law. Copyright and IPR is retained by the creators or other copyright holders. Terms and conditions for use of this material are defined in the [End User Agreement](#).

www.reading.ac.uk/centaur

CentAUR

Central Archive at the University of Reading

Reading's research outputs online

1 Skill of seasonal rainfall and temperature forecasts for East Africa

2

3 Hannah R. Young* and Nicholas P. Klingaman

4

5 National Centre for Atmospheric Science–Climate and Department of Meteorology,

6 University of Reading, Reading, UK

7

8 *Corresponding author. Email hannah.young@reading.ac.uk

9

10

11

12

13

14

15

16

17

18

19

20

21

22

23

24 **Abstract**

25 Skilful seasonal forecasts can provide useful information for decision makers,
26 particularly in regions heavily dependent on agriculture, such as East Africa. We
27 analyse prediction skill for seasonal East African rainfall and temperature one to four
28 months ahead from two seasonal forecasting systems: the US National Centers for
29 Environmental Prediction (NCEP) Coupled Forecast System Model Version 2
30 (CFSv2) and the UK Met Office (UKMO) Global Seasonal Forecast System Version
31 5 (GloSea5). We focus on skill for low or high temperature and rainfall, below the
32 25th or above the 75th percentile respectively, as these events can have damaging
33 effects in this region. We find skill one month ahead for both low and high rainfall
34 from CFSv2 for December-January-February in Tanzania, and from GloSea5 for
35 September-October-November in Kenya. Both models have higher skill for
36 temperature than for rainfall across Ethiopia, Kenya and Tanzania, two months
37 ahead in some cases. Performance for rainfall and temperature change in the two
38 models during certain El Niño Southern Oscillation (ENSO) and Indian Ocean Dipole
39 (IOD) phases, the impacts of which vary by country, season and sometimes by
40 model. While most changes in performance are within the range of uncertainty due
41 to the relatively small sample size in each phase, they are significant in some cases.
42 For example, La Niña lowers performance for Kenya September-October-November
43 rainfall in CFSv2 but does not affect skill in GloSea5.

44

45

46

47 **1. Introduction**

48 Forecasts of rainfall and temperature for upcoming months can be valuable for
49 decision makers to anticipate and mitigate the effects of unfavourable conditions.
50 Forecast information can guide the decisions of policymakers in agriculture and food
51 security, water management, disaster risk reduction, emergency relief and health
52 (Lemos et al., 2002; Vitart et al., 2012), and at local scales be useful for subsistence
53 farmers (Patt and Gwata, 2002; Hansen et al., 2011). East Africa is particularly
54 vulnerable to the effects of rainfall and temperature extremes, as much of the
55 population depends on rainfed agriculture for their income: 79% in Ethiopia, 77% in
56 Tanzania and 61% in Kenya (FAO, 2018). Crops and livestock can be affected by
57 heat stress, drought conditions (Herrero et al., 2010), and frosts (Kotikot and
58 Onywere, 2015), and the prevalence of disease is also influenced by both rainfall
59 and temperature (Bandyopadhyay et al., 2012).

60

61 For forecasts to be successfully interpreted and applied in this region, it is necessary
62 to understand the skill and reliability of ensemble forecasting systems for predicting
63 rainfall and temperature on decision-relevant timescales. Seasonal rainfall variability
64 over the East African region is influenced by local factors such as topography,
65 coastal influences and lakes; regional circulation drivers such as the tropical easterly
66 jet; and remote drivers such as the El Niño–Southern Oscillation (ENSO), the Indian
67 Ocean Dipole (IOD) and the Madden-Julian Oscillation (MJO) (Nicholson, 2017).
68 Successful rainfall predictions rely on the ability of seasonal forecast models to
69 represent a range of drivers and their relationships to regional rainfall. Models also

70 need to capture the seasonal cycle of rainfall. While some parts of the region
71 experience one rainy season per year, such as southern Tanzania and northern
72 Ethiopia, the near-equatorial region including northern Tanzania, Kenya and
73 southern Ethiopia has two rainy seasons (Dunning et al., 2016; Nicholson, 2017).
74 Successful temperature predictions also rely on models representing drivers, both
75 local and remote, and their relationships to regional conditions. In particular, soil
76 moisture conditions and ENSO phase are important for predicting heatwaves
77 (Hirschi et al., 2011; Russo et al., 2016; van den Hurk et al., 2010).

78

79 *a. Seasonal forecasts for East Africa*

80

81 Nicholson (2017) provides a comprehensive overview of previous work on the skill of
82 seasonal rainfall forecasts over eastern Africa. The short rains (October to
83 November) are generally more predictable than the long rains (March to May),
84 particularly in dynamical models. In both seasons statistical models are generally
85 more skilful than dynamical ones, however dynamical models do outperform in some
86 cases. For instance, Walker et al. (2019) found a dynamical model had higher skill
87 for predicting East African rainfall than a consensus forecast based on both
88 statistical and dynamical models.

89

90 Statistical models identify remote atmospheric and oceanic drivers with
91 teleconnections to the region of interest, to predict conditions in the coming months.
92 These models therefore rely on the availability of information about the relevant
93 drivers ahead of the season of interest to make a prediction. For example, Camberlin

94 and Philippon (2002) used observed ENSO and other predictors identified using
95 principal component analysis to predict March to May rainfall in East Africa. Diro et
96 al. (2008, 2011) developed skilful statistical forecasts for Ethiopia's spring and
97 summer rains based on teleconnections from sea surface temperatures (SSTs) in
98 regions across the globe. Funk et al. (2014) used western central Pacific and central
99 Indian Ocean SSTs to predict East African droughts and Chen and Georgakakos
100 (2015) forecast East African rains using SST dipoles across basins including the
101 Mediterranean Sea, North and South Atlantic, Indian Ocean, and Arabian Sea.

102

103 Nicholson (2014) produced regression models based on SST, sea level pressure
104 and vertical and horizontal winds at different heights to predict March-April-May,
105 July-August-September and October-November rains in equatorial and summer
106 rainfall regions. The summer rainfall region was defined by areas of East Africa
107 where the maximum rainfall falls between June and September, and the equatorial
108 rainfall region was defined where the maximum rainfall falls within March-April-May
109 or October-November. Correlations between modelled and observed rainfall were
110 above 0.76 up to five months ahead for October-November rainfall in both regions,
111 two months ahead for July-August-September rainfall in the summer rainfall region,
112 and two months ahead for March-April-May rainfall in the equatorial region. This
113 highlighted how the ENSO spring predictability barrier (Webster and Yang, 1992)
114 can hinder prediction of spring and summer rains at longer lead times (Nicholson,
115 2017). Along with later work (Nicholson, 2015), the Nicholson (2014) study also
116 found that statistical models that used atmospheric variables on multiple levels as
117 predictors tended to have higher skill than those that used only surface variables.

118

119 On the other hand, dynamical forecasts are predictions from models that represent
120 the physical processes underlying weather and climate. While dynamical systems
121 are generally less skillful than statistical models over East Africa (Nicholson, 2017),
122 they are increasingly being developed and used, and there is evidence of skill for
123 predicting seasonal temperature (Weisheimer and Palmer, 2014) and rainfall
124 (Bahaga et al., 2016; Batté and Déqué, 2011; Diro et al., 2012; Dutra et al., 2013;
125 MacLeod, 2018; Mwangi et al., 2014; Walker et al., 2019). In this paper we will
126 contribute to greater understanding of the skill of two contemporary dynamical
127 seasonal forecasting systems, the US National Centers for Environmental Prediction
128 (NCEP) Coupled Forecast System Model Version 2 (CFSv2, Saha et al., 2014) and
129 the UK Met Office (UKMO) Global Seasonal Forecast System Version 5 (GloSea5,
130 MacLachlan et al., 2015).

131

132 We focus on the skill of CFSv2 and GloSea5 for high or low rainfall or temperature
133 for countries in East Africa, with lead times of one to four months. While GloSea5
134 rainfall forecasts have been analysed by Walker et al. (2019) across East Africa at
135 one month lead time for tercile event categories, here we analyse additionally lead
136 times out to four months, to determine how far ahead useful predictions can be
137 made. We also evaluate temperature forecasts, as these may also be relevant for
138 decision-makers in the region, and we provide a comparison with CFSv2. In each
139 case we also analyse the forecasts at country-scale, which has not been done
140 before for these models. Alongside information at both larger regional and smaller
141 sub-national scales, forecasts for individual countries may be useful for decision

142 makers advising at this scale, such as humanitarian agencies, so an understanding
143 of country-level skill is relevant in this context. We compare skill over Ethiopia,
144 Kenya and Tanzania, three relatively large countries in the East Africa region with
145 different seasonal cycles, particularly for rainfall.

146

147 In the next section we describe the data and methods used in this study. We present
148 results in section 3 and in section 4 we discuss these in the context of skill of other
149 models and future research opportunities.

150 **2. Data and Methods**

151 *a. Re-forecast and observational data*

152

153 The re-forecast data are from the NCEP CFSv2 and UKMO GloSea5 models. CFSv2
154 re-forecasts are started every five days starting from the 1st of January, running for
155 nine months, for the period 1982-2011. They have four ensemble members and
156 T126 resolution (approximately 100km). GloSea5 re-forecasts are started on the 1st,
157 9th, 17th and 25th of each month, with seven ensemble members, and are run for
158 approximately seven months (216 days). We used re-forecasts for 1993-2015 at
159 N216 resolution (approximately 60km at midlatitudes). For each model, all re-
160 forecasts within a calendar month were merged to produce larger ensembles of re-
161 forecasts, and for ease of comparing the models. This resulted in an ensemble size
162 of either 20, 24 or 28 for CFSv2 (four ensemble members started on either 5, 6 or 7
163 start dates, depending on the month), and an ensemble size of 28 for GloSea5 (7
164 ensemble members started on 4 start dates). We evaluate both models at lead times

165 of one to four months. The lead time corresponds to the time ahead of the start of
166 the season. For example, re-forecasts for DJF at one month lead are those starting
167 on any dates in November; re-forecasts at four months lead are those starting on
168 any dates in August.

169

170 Rainfall data to validate the re-forecasts are taken from the Global Precipitation
171 Climatology Project (GPCP; Adler et al., 2003) at 2.5 x 2.5 degree resolution
172 (approximately 275km at the equator). Temperature data are near-surface (2 metre)
173 air temperatures from the ECMWF Interim reanalysis (ERA-Interim; Dee et al., 2011)
174 at N128 resolution (approximately 80km). Model data were regridded to the grid of
175 the observations for gridpoint scale analyses.

176

177 *b. Methods*

178

179 We analysed the re-forecasts over the standard meteorological seasons (DJF, MAM,
180 JJA, SON), with lead times one to four months ahead of the season of interest.

181 Analyses were carried out at gridpoint scale and at country-average scale. Results
182 are shown at country scale as, due to geopolitical considerations, information at this
183 scale is sometimes used to guide decisions in humanitarian or other sectors. Results
184 are shown for DJF and JJA for temperature, and for the main rainy seasons in each
185 country. It is meteorological practice in Ethiopia to partition rainfall in three four-
186 month seasons: FMAM, JJAS (the main rainy season) and ONDJ. For consistency
187 with the analysis for other countries we here retain use of three-month periods and

188 focus on the two seasons where these are a subset of the longer seasons: JJA and
189 MAM.

190

191 Biases in the mean of the forecasts compared to the observations were first
192 calculated. Mean biases for each lead time (in weeks) were then removed from the
193 hindcasts before the rest of the analysis was carried out. Anomaly Correlation
194 Coefficients (ACC) were also calculated for the ensemble mean, which is the
195 correlation between the forecasts and observations, each taken as an anomaly from
196 their own climatology. These are temporal correlations, and are calculated both at
197 gridpoint and country scale.

198

199 We also calculated the Brier Skill Score (BSS), to compare the skill of the re-
200 forecasts to a climatological forecast. We use a climatological forecast that always
201 forecasts the expected likelihood of an event, e.g. events below the 25th percentile
202 are expected to occur 25% of the time, so are forecast with probability 0.25. The
203 Brier Skill Score is

204
$$BSS = 1 - \frac{BS}{BS_{ref}}$$

205 where BS is the Brier Score of the forecast and BS_{ref} is the Brier Score of a
206 reference (climatological) forecast. The Brier Score is defined as

207
$$BS = \frac{1}{N} \sum_{t=1}^N (f_t - o_t)^2$$

208

209 where N is the number of forecasts, f_t are the forecast probabilities of an event and o_t
210 are the indicators of whether the event was observed (1 if it occurred; 0 if it did not
211 occur), at each forecast instance t . A BSS above 0 indicates skill greater than that of
212 a climatological forecast. Finally, reliability diagrams were also produced, comparing
213 the forecast probability of an event with its observed frequency. Using five bins to
214 partition the forecast probabilities, the observed relative frequency for each bin is
215 plotted against the average probability value of all forecasts within the bin (Bröcker
216 and Smith, 2007). Reliability is shown aggregated over leads of one to two months
217 and three to four months. Both BSSs and reliability diagrams were calculated using
218 country-averaged predicted and observed rainfall and temperature.

219

220 BSSs and reliability diagrams were calculated for events below the 25th percentile,
221 between the 25th and 75th percentiles, and above the 75th percentile. These were
222 calculated using percentiles based on the re-forecast rainfall and temperature
223 distributions (e.g. f_t = forecast probability of an event above the re-forecasts' 75th
224 percentile, o_t =whether observations were above the observations' 75th percentile),
225 as this calibrates for errors in the models' distributions of rainfall and temperature.
226 Re-forecast percentiles were calculated for each lead time (in months) for the BSS
227 and reliability calculations. To estimate uncertainty in the BSSs, the original
228 ensemble for each year was bootstrapped 1000 times, sampling with replacement to
229 produce ensembles the same size as the original. The re-forecast percentiles were
230 recalculated each time along with the BSS in order to establish the 5th and 95th
231 percentiles of the uncertainty range.

232 Biases and ACCs were also compared for different El Niño Southern Oscillation
233 (ENSO, Trenberth, 1997) and Indian Ocean Dipole (IOD, Saji et al., 1997) phases,
234 as these large scale circulation changes have teleconnections to East Africa (e.g.
235 Ropelewski and Halpert, 1987; Nicholson and Kim, 1997; Black et al., 2003; Black,
236 2005) and may affect forecast skill (e.g. Goddard and Dilley, 2005). ENSO indices
237 were retrieved from NOAA and IOD indices from JAMSTEC. Tercile categories were
238 used to determine negative (below 33rd percentile), neutral (between 33rd and 66th
239 percentile) and positive (above 66th percentile) years for each season. Forecasts
240 were then categorised using the observed IOD and ENSO indices for the season.
241 Biases are shown for these subsets, averaging over 11 (La Niña, positive and
242 negative IOD) or 12 (El Niño) years for the observations, 10 years for CFSv2 and 8
243 years for GloSea5. In order to estimate whether the conditional ACCs for ENSO and
244 IOD phases lie outside the range of sampling uncertainty, the original uncategorised
245 ensemble was also bootstrapped 1000 times. Each time the same number of years
246 were sampled as were in the ENSO or IOD tercile categories (10 for CFSv2 and 8
247 for GloSea5) and the ACC calculated, in order to establish the 5th and 95th
248 percentiles of the sampling uncertainty range.

249

250 **3. Results**

251 *a. Model biases*

252

253 Rainfall results for MAM and SON show that both models have clear mean-state
254 rainfall biases over East Africa (Fig. 1a). CFSv2 has a dry bias in MAM in regions of

255 observed high rainfall, and in SON there is a dry bias across the western part of the
256 region. These biases increase slightly from lead-1 to lead-3. CFSv2 also produces
257 wet biases in the northern Ethiopian highlands of up to 3mm/day, suggesting the
258 simulated rainfall is too sensitive to orography. GloSea5 rainfall biases are much
259 smaller in MAM. In SON, GloSea5 has a wet bias of over 3mm/day across the
260 region, corresponding to the wet bias found by Walker et al. (2019) for the OND
261 season. The wet bias increases slightly from lead-1 to lead-3. Both models also
262 show large rainfall biases over the Indian Ocean. CFSv2 interannual rainfall
263 variability is generally too low across East Africa, while GloSea5 has too little
264 variance where observed variance is high, but too much variance in other parts of
265 the region (not shown).

266

267 Temperatures vary little throughout the year in Ethiopia, Kenya and Tanzania (Fig.
268 1b). CFSv2 is too cool over the Horn of Africa, and additionally over Tanzania and
269 the southern part of the region in JJA, but too warm into central Africa. Temperatures
270 over Ethiopia, Kenya and Tanzania are mostly up to 2°C too cool and these biases
271 change little with lead time. GloSea5 is too cool by up to 5°C in the northern part of
272 the region and too warm across the southern part in DJF, and in JJA the warm bias
273 is further north and includes Ethiopia, with biases above 2°C. There is also a strong
274 warm bias over Lake Victoria. The biases over Ethiopia, Kenya and Tanzania
275 change little with lead time but the warm bias over central Africa in JJA decreases
276 from lead-1 to lead-3. Both models also have variability which is too high where
277 observed variance is low, and too low where observed variance is high (not shown).

278

279 1) BIASES CONDITIONED ON ENSO AND IOD

280

281 Rainfall and temperature in East Africa are affected by SST variations in the ENSO
282 and IOD regions. Fig. 2a shows that observed rainfall in SON over Kenya and
283 Tanzania is generally above-normal in El Niño and positive IOD phases, by up to 0.8
284 mm/day, while in negative IOD rainfall is up to 0.6 mm/day below-normal. In MAM
285 changes are smaller, but there is slightly above normal rainfall in Ethiopia during El
286 Niño, and across all three countries during negative IOD. During positive IOD events
287 there is below normal rainfall over the region. ENSO and IOD teleconnections to
288 MAM rainfall are generally weak (e.g. Liebmann et al., 2014; Mutai and Ward, 2000;
289 Vellinga and Milton, 2018), however the effects seen here are likely due to the tercile
290 SST categories defined over a relatively short time period. Conditional rainfall biases
291 in CFSv2 (biases in SST phases relative to the bias in all years) are based on only
292 10 years of data but remain similar in MAM (Fig. 2b) to the unconditional biases (i.e.,
293 all years), although the dry bias is increased in negative IOD. In SON, the dry bias
294 over Kenya is amplified during El Niño and positive IOD events, but decreased
295 during the opposite phases. Fig. 2c shows GloSea5 rainfall biases, which are based
296 on only 8 years of data, appear to change relatively little with ENSO and IOD phase
297 in MAM. However in SON the wet bias over the region is increased during La Niña
298 and negative IOD events, but reduced during El Niño and positive IOD phases.

299

300 Fig. 3a shows that in El Niño and positive IOD phases, the East African region
301 generally experiences warm anomalies in JJA, particularly over Ethiopia which is up
302 to 0.8°C warmer during El Niño. The region is cooler in JJA during La Niña, while

303 differences in DJF are smaller across the phases. CFSv2 has conditional
304 temperature biases largely similar to the unconditional biases over the East African
305 region (Fig. 3b). Fig. 3c shows conditional biases are also similar to unconditional
306 biases in GloSea5, however the cool bias over Ethiopia and Kenya in DJF is slightly
307 reduced in El Niño and positive IOD years and amplified in the opposite phases.
308 Again these biases are based on small sample sizes.

309

310 *b. Regional performance*

311

312 Fig. 4 shows the Anomaly Correlation Coefficients (ACC) for precipitation and
313 temperature at leads 1 and 3 for the ensemble means of the two models. ACCs are
314 lower for rainfall than temperature for both models. For MAM, CFSv2 has rainfall
315 ACC values above 0.4 over northern Ethiopia at lead-1, but by lead-3 these values
316 have decreased, and there is no significant correlation between the model and the
317 observations over Kenya and Tanzania (Fig. 4a). In SON, ACC values are above 0.4
318 over eastern Ethiopia and Kenya and above 0.2 across Tanzania at lead-1, and
319 these decrease over the eastern part of the region by lead-3. GloSea5 ACCs show
320 similar spatial patterns across the countries of interest in MAM, but with higher
321 magnitudes at lead-1 than CFSv2, particularly over Kenya. However in SON the
322 region over eastern Ethiopia and Kenya has higher ACC values than CFSv2 at lead-
323 1, at over 0.6, and this extends out to lead-3. The region of high correlation over land
324 in GloSea5 is broadly similar to the equatorial region analysed by Nicholson (2014),
325 whose regression model had a correlation of 0.78 with observations at 2 months
326 lead.

327

328 ACCs for DJF temperature in CFSv2 are positive over Ethiopia, Tanzania and parts
329 of Kenya, with particularly high values over 0.6 in northern Ethiopia at both lead-1
330 and lead-3 (Fig. 4b). JJA results are similar, but with higher correlation over Kenya at
331 lead-1 and lower correlation across Ethiopia and Tanzania at lead-3. GloSea5
332 results for JJA temperature also show positive ACCs across most of the region, with
333 values above 0.6 over Tanzania out to lead-3. Lower ACCs are found in DJF, and
334 particularly over parts of Kenya there is no significant correlation between the model
335 and the observations as is the case in CFSv2.

336

337 This analysis is based on different time periods for the two models to make full use
338 of the available data and maximise the sample size. However when using the same
339 time period for both models (1993-2011), the spatial patterns of the ACCs are very
340 similar (Fig. S1 in Supplemental Material). While there are some regions where the
341 magnitude decreases, for example GloSea5 JJA temperature ACCs over Kenya and
342 Tanzania are slightly lower when the shorter time period is used, overall these
343 changes are small.

344

345 *c. Country-level skill: Ethiopia*

346

347 For country-level skill, Figures 5-12 show results for leads 1-4, while Tables 1 and 2
348 provide significance testing for lead-1 and lead-2.

349

350 We analyse the skill for forecasts averaged over Ethiopia for key 3-month seasons.
351 The CFSv2 rainfall ACC is 0.48 at lead-1 for JJA, but for MAM ACCs are lower and
352 not significant at lead-1 (Fig. 5a, Table 1). ACCs decrease with lead time out to lead-
353 4 in MAM and lead-3 in JJA. In El Niño and positive IOD phases CFSv2 ACCs are
354 higher than the unconditioned ACC in MAM, and lower in the opposite phases. The
355 conditioned ACC only lies outside the 5th to 95th percentile uncertainty range from
356 bootstrapping the original ensemble for negative IOD years at lead-1 and lead-2,
357 suggesting that the difference is significant at the 90% confidence level at these
358 leads. GloSea5 ACC values are slightly higher than those from CFSv2 in JJA out to
359 lead-3, and are also much lower and not significant in MAM (Fig. 5a, Table 1). ACCs
360 are higher in La Niña and negative IOD phases in JJA, although this lies within the
361 range of uncertainty. CFSv2 rainfall BSS values are around 0 for all event categories
362 in both seasons, except for dry events (below 25th percentile) at lead-2 in JJA where
363 the BSS and its uncertainty range is positive, showing a slight improvement over a
364 climatological forecast (Fig. 6a, Table 1). GloSea5 BSS values are also very close to
365 0, indicating no improvement over a climatological forecast. Reliability curves from
366 CFSv2 and GloSea5 for rainfall generally show little change with lead time, and are
367 closest to the 1:1 line in both models for wet events in MAM and dry events in JJA,
368 signifying that forecast probabilities correspond well to the observed frequencies of
369 events (Fig. 7a). Reliability for average (25th-75th percentile) events is poor in MAM
370 for both models (Fig. S2a, S3a in Supplemental Material).

371

372 ACCs for temperature are higher than for rainfall in both models, and remain around
373 0.5 for all lead times in DJF but decrease with lead time in JJA, from 0.66 in CFSv2

374 and 0.88 in GloSea5 (Fig. 9a, Table 2). La Niña and negative IOD phases have
375 higher ACCs in DJF in CFSv2, while positive IOD ACCs are negative and outside the
376 range of uncertainty. El Niño leads to higher ACCs in DJF and JJA in GloSea5,
377 however this conditional ACC does not lie outside the uncertainty range, suggesting
378 the difference is not significant. CFSv2 BSSs and their uncertainty ranges are
379 positive for cool (below 25th percentile) events in DJF at all lead times, and warm
380 events (above 75th percentile) in JJA at lead-1 (Fig. 10a, Table 2). GloSea5 BSSs
381 and their uncertainty ranges are positive at lead-1 and lead-2 for average events in
382 DJF and warm events in JJA, and at lead-1 for average events in JJA. Reliability
383 diagrams for temperature from CFSv2 show slight improvement from lead 3-4 to lead
384 1-2, and match the 1:1 line reasonably well for cool events in DJF and JJA and warm
385 events in JJA, but they tend to be too shallow (Fig. 11a). Reliability diagrams for
386 GloSea5 (Fig. 12a) show a similar picture. For the average (25th-75th percentile)
387 category, CFSv2 forecast probabilities showing little relationship with the observed
388 frequencies, but curves are close to the 1:1 line in GloSea5, particularly for DJF (Fig.
389 S4a, S5a in Supplemental Material).

390

391 *d. Country-level skill: Kenya*

392

393 Kenya receives most rainfall in MAM and SON. CFSv2 has slightly higher
394 correlations in MAM than SON, while GloSea5 ACC values are slightly higher than
395 CFSv2 at lead-1 for MAM, and much higher for SON with ACCs above 0.7 out to
396 lead-2 (Fig. 5b, Table 1). El Niño has a strong forcing on SON rainfall in East Africa,
397 and is associated with above normal conditions (Black, 2005). Separating out years

398 into ENSO and IOD phases suggests that CFSv2 and GloSea5 have consistently
399 greater performance in El Niño years in SON, however this is within the range of
400 uncertainty. While GloSea5 has a slight decrease in performance in La Niña years in
401 SON, CFSv2 exhibits a much greater decrease that consistently lies outside the
402 uncertainty range and the model is strongly anti-correlated with the observations by
403 lead-3 (Fig. 5b). CFSv2 BSS values are very close to 0 for all events and lead times
404 (Fig. 6b, Table 1), showing skill similar to climatological forecast skill. GloSea5 skill is
405 above that of a climatological forecast at lead-1 for wet events in MAM and SON and
406 dry events in SON (Fig. 6b, Table 1). CFSv2 rainfall reliability changes little with lead
407 time and is best for dry events in MAM and wet events in SON (Fig. 7b). GloSea5
408 reliability curves are particularly close to the 1:1 line for wet events in SON out to
409 lead 3-4 (Fig. 8b). Reliability for average events is better in CFSv2 for MAM and
410 GloSea5 for SON (Fig. S2b, S3b in Supplemental Material).

411

412 CFSv2 temperature ACC values remain around 0.5 at all lead times in JJA, and are
413 slightly lower in DJF (Fig. 9b, Table 2). GloSea5 ACCs are lower than CFSv2 in DJF
414 but similar in JJA. ACCs in negative IOD phases are slightly greater than in all years
415 in JJA in both models, and outside the range of uncertainty at longer lead times in
416 both. CFSv2 also has much lower ACCs with negative correlations during positive
417 IOD years in JJA. CFSv2 has positive BSSs, showing an improvement over a
418 climatological forecast, for cool events in DJF at lead-1 and in JJA at lead-1 and
419 lead-2 (Fig. 10b, Table 2). GloSea5 has BSSs above zero only for warm events in
420 JJA at lead-1 and lead-2. Reliability for temperature from CFSv2 is best for cool
421 events in JJA at leads 1-2, whereas curves for warm events are too shallow (Fig.

422 11b). GloSea5 reliability is poor, particularly for cool events (Fig. 12b). Reliability is
423 generally poor for average events, although the curve at lead 1-2 for JJA in CFSv2 is
424 close to the 1:1 line (Fig. S4b, S5b in Supplemental Material).

425

426 *e. Country-level skill: Tanzania*

427

428 In Tanzania in DJF, both models have ACCs for rainfall above 0.5 at lead-1; this
429 decreases with lead time in CFSv2 but remains fairly constant in GloSea5 (Fig. 5c,
430 Table 1). ACCs are much lower in both models in MAM, and are mostly around or
431 below zero. ENSO and IOD phase has little consistent effect on the ACC in DJF in
432 either model, but generally ACCs are lower in negative IOD than the unconditioned
433 case. In MAM, La Niña increases the ACC at all lead times in both models, but this is
434 within the sampling uncertainty range. El Niño decreases skill in MAM in out to lead-
435 3 in both models, and this is outside the range of uncertainty at lead-1. CFSv2 has
436 positive BSSs for dry and wet events at lead-1 in DJF, but other events and leads
437 are close to or below 0 (Fig. 6c, Table 1). The uncertainty range of GloSea5 BSSs at
438 lead-1 and lead-2 does not lie above 0 in either season (Fig. 6c). CFSv2 reliability
439 curves are close to the 1:1 line for dry events in DJF, and wet events in DJF at lead
440 1-2 (Fig. 7c). Reliability for rainfall is also better in GloSea5 in DJF than MAM, where
441 dry and wet events are both only predicted with low probabilities (Fig. 8c). For
442 average events, forecast probabilities show little relationship with observed
443 frequencies in CFSv2, but the curve is close to the 1:1 line in DJF at lead 1-2 in
444 GloSea5 (Fig. S2c, S3c in Supplemental Material).

445

446 Temperature ACCs are around 0.5 at lead-1 for both seasons in CFSv2, and
447 decrease slightly with lead time (Fig. 9c, Table 2). ACCs are lower in DJF in
448 GloSea5 than in CFSv2, but higher in JJA. ENSO and IOD phase influences on the
449 ACCs mostly lie within the range of uncertainty. Both models show slight
450 improvements in negative IOD years in JJA, and there is a decrease in ACC when in
451 El Niño phase for JJA in CFSv2 which does lie outside the range of sampling
452 uncertainty. BSS values and their uncertainty ranges are positive in CFSv2 at lead-1
453 and lead-2 for cool events in DJF and cool and average events in JJA, and at lead-1
454 for warm events in DJF (Fig. 10c, Table 2), signifying higher skill than a
455 climatological forecast. GloSea5 has less skill over Tanzania in DJF, with negative
456 BSS values for lead-1 for all temperature categories, but higher skill than a
457 climatological forecast at lead-1 and lead-2 for cool and warm events in JJA.
458 Reliability diagrams for temperature from CFSv2 and GloSea5 show curves are
459 closest to the 1:1 line for warm events in DJF and cool events in JJA at lead 1-2 (Fig.
460 11c, 12c). Reliability for average events is better for JJA than DJF in both models
461 (Fig. S4c, S5c in Supplemental Material).

462 **4. Discussion and conclusions**

463 *a. Rainfall skill*

464

465 Country ACCs and BSSs for rainfall forecasts at leads 1 and 2 are summarised in
466 Table 1. CFSv2 temperature anomalies significantly correlate with observations only
467 at lead-1 in JJA in Ethiopia, and lead-1 and lead-2 in MAM in Kenya and DJF in
468 Tanzania. Skill is mostly similar to that of a climatological forecast, only showing

469 improvement above this at lead-1 for dry and wet events in DJF in Tanzania, and at
470 lead-2 for dry events in JJA in Ethiopia.

471

472 GloSea5 skill is generally similar to CFSv2 for rainfall, also having positive anomaly
473 correlations for JJA in Ethiopia, MAM in Kenya and DJF in Tanzania. However
474 GloSea5 also has strong correlations for SON rainfall in Kenya at both lead-1 and
475 lead-2. Skill is only above that of a climatological forecast for wet events in MAM and
476 wet and dry events in SON in Kenya at lead-1.

477

478 Both models have similar skill for average events to a climatological forecast.

479 Average events are mostly forecast by around 50% of ensemble members (Fig. S2,
480 S3 in Supplemental Material), which matches the definition of occurring 50% of the
481 time. This indicates the models have low sharpness - the ability to generate forecast
482 probabilities that are different to the climatological frequency of the event. Where the
483 models do exhibit skill above that of a climatological forecast this is for below normal
484 and above normal rainfall events. This is similar to results from Diro et al. (2008,
485 2011) for a statistical model based on SST anomalies, and from Walker et al. (2019)
486 for GloSea5 which found higher skill for the outer tercile categories over a large East
487 Africa region. In these skilful cases, the models predict the events with probabilities
488 that are different to the 25% frequency defining dry and wet events, demonstrating
489 sharpness. For example, CFSv2 has skill for dry and wet events in Tanzania in DJF,
490 and GloSea5 has skill for dry and wet events in Kenya in SON. In both of these
491 cases the distribution of forecast probabilities at lead 1-2 peaks at the lowest values,
492 suggesting a high frequency of forecasts giving less than climatological chances of

493 the events, along with some forecasts giving probabilities above 25% (Figure 7,
494 Figure 8).

495

496 Walker et al. (2019) found skill for the short rains (OND) over East Africa in GloSea5
497 at one month ahead, particularly for upper tercile events, along with an increase in
498 skill and reliability of East African rainfall when GloSea5 forecasts an IOD event.

499 ECMWF System 4 also has good rainfall reliability in this region (Weisheimer and
500 Palmer, 2014). The reliability in these analyses appears consistent with the reliability
501 results shown here, in particular for wet events in SON in Kenya. Differences in the
502 reliability from these previous studies are likely to be because here the country-
503 average has been used, rather than an aggregation over the gridpoints in each
504 region. This does mean the sample sizes are smaller, making the reliability estimates
505 less robust and more susceptible to random variations due to undersampling,
506 however the estimates still support those from Walker et al. (2019).

507

508 Forecasts for the long rains season (MAM) have been shown to be generally less
509 skilful than forecasts for the short rains (ON, e.g. Nicholson, 2014; Nicholson, 2017;
510 MacLeod, 2018). ACC results in Fig. 4a show that over the East Africa region
511 GloSea5 has greater correlation in SON than in MAM over the eastern part of the
512 region, however CFSv2 at lead-1 has greater performance for MAM than SON over
513 Ethiopia and Kenya. This is reflected in the country scale results, where ACC values
514 for Kenya from CFSv2 are higher in MAM than SON, but values from GloSea5 are
515 higher in SON (Table 1). GloSea5 also has positive BSSs for dry and wet events in

516 SON and wet events in MAM in Kenya (Table 1), which suggests this model may be
517 able to provide skilful forecast information particularly for the short rains season.

518

519 *b. Temperature skill*

520

521 Country ACCs and BSSs for temperature forecasts at leads 1 and 2 are summarised
522 in Table 2. Temperature forecast skill is generally higher than rainfall, with more
523 significant ACCs and BSS uncertainty ranges above zero in both models. CFSv2
524 ensemble mean temperature anomalies significantly positively correlate with
525 observed anomalies at lead-1 for all countries and seasons, and at lead-2 for all
526 except DJF in Kenya. CFSv2 has skill at predicting cool events in all countries, with
527 the uncertainty above zero indicating skill above that of a climatological forecast in all
528 seasons except JJA in Ethiopia, and mostly out to lead-2. Skill is lower for normal
529 events, where it is only above a climatological forecast for JJA in Tanzania, and for
530 warm events where it is only above for JJA in Ethiopia and DJF in Tanzania at lead-
531 1.

532

533 GloSea5 temperature anomaly correlations are higher than CFSv2 for JJA in all
534 countries at lead-1 and lead-2, positive and similar to CFSv2 for DJF in Ethiopia, but
535 not significant for DJF in Kenya and Tanzania. Skill for cool events is lower than
536 CFSv2, with skill above a climatological forecast only for JJA in Tanzania. However,
537 GloSea5 has skill for normal events at lead-1 in DJF and JJA in Ethiopia where
538 CFSv2 does not, and has skill for warm events at lead-1 and lead-2 in JJA in all
539 three countries.

540

541 Both CFSv2 and GloSea5 have some skill at predicting temperatures in East Africa
542 at 1 and 2 month lead times, CFSv2 particularly for cool events and GloSea5
543 particularly for warm events in JJA. Few other studies have analysed seasonal
544 temperature forecast skill over this particular region. However ECMWF System 4 has
545 been shown to have good reliability for warm (upper tercile) and cold (lower tercile)
546 DJF and JJA seasons over a large East African region one month ahead
547 (Weisheimer and Palmer, 2014). Combined with the results shown here this
548 suggests that dynamical models are able to make skilful and reliable temperature
549 predictions for this region in some seasons.

550

551 *c. Limitations and future opportunities*

552

553 In this study skill and reliability may be limited by the size of the reforecast datasets
554 (30 years for CFSv2 and 23 years for GloSea5), particularly when the record is split
555 into ENSO and IOD phases; most of the differences between conditional and
556 unconditional performance were not significant. Results may also be sensitive to the
557 time periods which do not match between the models. A much longer re-forecast set
558 would be required to have enough years in each ENSO and IOD phase to
559 substantially reduce uncertainty; around 20 years are currently used to characterise
560 seasonal forecast skill so this may need to be up to three times as long.

561

562 The impact of ENSO and IOD phase on prediction performance is often consistent
563 across the two models. For example, increased skill for MAM rainfall in Kenya in

564 positive IOD years and JJA temperature in Tanzania in negative IOD years. However
565 impacts do differ across the two models in some countries and seasons. For
566 example for JJA rainfall in Ethiopia, negative IOD phase improves performance in
567 GloSea5 but has little effect in CFSv2, while for SON rainfall in Kenya, La Niña
568 significantly decreases skill in CFSv2 but has little effect in GloSea5. For JJA
569 temperature in Kenya, La Niña increases skill in CFSv2 but decreases skill in
570 GloSea5, while positive IOD phase significantly decreases skill in CFSv2 but has
571 little impact in GloSea5. Many of the impacts in both models are within the range of
572 sampling uncertainty. With a limited sample size, it is difficult to rule out the effect of
573 other influences and isolate the role of ENSO and IOD. While terciles are used for
574 ENSO and IOD categorisation in each season so there are equal numbers of years
575 in each phase, SST variability is likely to be higher in some seasons, for example El
576 Niño and La Niña events typically peak in DJF, and there may be stronger influences
577 on rainfall in certain seasons. Longer reforecast datasets would aid more robust
578 estimates of changes in performance and skill based on the phase of ENSO and IOD
579 variability.

580

581 Bahaga et al. (2016) showed that a realistic representation of the relationship with
582 the Indian Ocean Dipole is important in capturing the variability of the rains in East
583 Africa. Walker et al. (2019) found GloSea5 represents the correlations between East
584 African rainfall and ENSO and IOD region SSTs well, but may have atmosphere-
585 ocean coupling which is too weak. Further work should investigate the
586 teleconnections to East Africa in CFSv2, along with model skill at replicating the SST
587 changes in each year to also help understand why different ENSO and IOD phases

588 may improve skill in each model. There may also be limitations due to the
589 observational datasets used for validation; for example GPCP has been shown to
590 underestimate high rainfall intensities over the region (Dinku et al., 2007; Kimani et
591 al., 2017).

592

593 Further work should investigate skill for smaller countries in the East African region,
594 or for sub-national or trans-national regions with consistent meteorological conditions
595 (e.g., timing of the wet season). Our skill results may be artificially low due to
596 variations within our target countries in meteorological regimes, e.g. differing rainy
597 seasons in northern and southern Ethiopia (Dunning et al., 2016). Here we analysed
598 the country scale as these forecasts are applied in humanitarian contexts where
599 decisions are in some cases made at country scales for geopolitical reasons.

600 However, model biases and performance vary across countries (Fig. 1a, Fig. 4a), so
601 the country-scale may reduce skill where it is high only in parts of the countries.

602 Downscaling may also help improve skill in this region (Diro et al., 2012; Kipkogei,
603 2017).

604

605 In general, it still appears that statistical models, for example based on SST
606 anomalies, may provide better skill at forecasting rainfall over the region. An
607 important addition to the literature would be rigorous comparisons of statistical and
608 dynamical model forecasts for the region, which are currently lacking. Models such
609 as those from Chen and Georgakakos (2015) and Nicholson (2014, 2015) have been
610 shown to produce reliable and skilful forecasts out to months ahead using indices
611 such as wind, SST, and SLP. The results here show that forecasts for rainfall at

612 country scale are country, season and event category dependent and in many cases
613 skill is very similar to that of a climatological forecast. However both dynamical
614 models may provide useful information. In particular, CFSv2 has skill for dry and wet
615 events in DJF in Tanzania at lead-1, while GloSea5 has skill for wet events in MAM
616 and dry and wet events in SON in Kenya at lead-1 where CFSv2 does not.
617 Temperature forecast skill is generally higher than rainfall, out to lead-2 in some
618 cases from both CFSv2 and GloSea5. In particular, CFSv2 has skill for cool events
619 in both DJF and JJA while GloSea5 has skill for warm events in JJA. Further
620 understanding of the models analysed here would require investigating the
621 underlying causes of the differences in skill between the CFSv2 and GloSea5
622 models, for example through identifying common factors between years when one
623 model strongly outperforms the other, and comparing to other dynamical seasonal
624 forecasting systems.

625

626 **Acknowledgements**

627 Hannah Young was funded by a grant from the UK Department for International
628 Development, via the Science for Humanitarian and Emergency Assistance and
629 Response (SHEAR) programme. Nicholas Klingaman was funded by an
630 Independent Research Fellowship from the Natural Environment Research Council
631 (NE/L010976/1). The authors are grateful for productive discussions with Prof.
632 Andrew Charlton-Perez. The authors thank NCEP and the Met Office for providing
633 re-forecast data. Data storage and analysis facilities were provided by the JASMIN
634 facility (<https://www.jasmin.ac.uk>).

635 **References**

636 Adler, R. F., and Coauthors, 2003: The Version 2 Global Precipitation Climatology
637 Project (GPCP) Monthly Precipitation Analysis (1979-Present). *J. Hydrometeorol.*, **4**,
638 1147–1167, [https://doi.org/10.1175/1525-](https://doi.org/10.1175/1525-7541(2003)004%3C1147:TVGPCP%3E2.0.CO;2)
639 [7541\(2003\)004%3C1147:TVGPCP%3E2.0.CO;2](https://doi.org/10.1175/1525-7541(2003)004%3C1147:TVGPCP%3E2.0.CO;2).

640

641 Bahaga, T. K., F. Kucharski, G. M. Tsidu, and H. Yang, 2016: Assessment of
642 prediction and predictability of short rains over equatorial East Africa using a multi-
643 model ensemble. *Theor. Appl. Climatol.*, **123**, 637–649,
644 <https://doi.org/10.1007/s00704-014-1370-1>.

645

646 Bandyopadhyay, S., S. Kanji, and L. Wang, 2012: The impact of rainfall and
647 temperature variation on diarrheal prevalence in Sub-Saharan Africa. *Appl. Geogr.*,
648 **33**, 63–72, <https://doi.org/10.1016/j.apgeog.2011.07.017>.

649

650 Batté, L., and M. Déqué, 2011: Seasonal predictions of precipitation over Africa
651 using coupled ocean-atmosphere general circulation models: Skill of the
652 ENSEMBLES project multimodel ensemble forecasts. *Tellus A*, **63**, 283–299,
653 <https://doi.org/10.1111/j.1600-0870.2010.00493.x>.

654

655 Black, E., 2005: The relationship between Indian Ocean sea–surface temperature
656 and East African rainfall. *Philos. T. R. Soc. A.*, **363**, 43–47,
657 <https://doi.org/10.1098/rsta.2004.1474>.

658

659 Black, E., J. Slingo, and K. R. Sperber, 2003: An observational study of the
660 relationship between excessively strong short rains in coastal East Africa and Indian
661 Ocean SST. *Mon. Wea. Rev.*, **131**, 74–94, [https://doi.org/10.1175/1520-
662 0493\(2003\)131%3C0074:AOSOTR%3E2.0.CO;2](https://doi.org/10.1175/1520-0493(2003)131%3C0074:AOSOTR%3E2.0.CO;2).

663

664 Bröcker, J., and L. A. Smith, 2007: Increasing the reliability of reliability diagrams.
665 *Weather Forecast.*, **22**, 651–661, <https://doi.org/10.1175/WAF993.1>.

666

667 Camberlin, P., and N. Philippon, 2002: The East African March–May rainy season:
668 Associated atmospheric dynamics and predictability over the 1968–97 period. *J.*
669 *Climate*, **15**, 1002–1019, [https://doi.org/10.1175/1520-
670 0442\(2002\)015%3C1002:TEAMMR%3E2.0.CO;2](https://doi.org/10.1175/1520-0442(2002)015%3C1002:TEAMMR%3E2.0.CO;2).

671

672 Chen, C.-J., and A. P. Georgakakos, 2015: Seasonal prediction of East African
673 rainfall. *Int. J. Climatol.*, **35**, 2698–2723, <https://doi.org/10.1002/joc.4165>.

674

675 Dee, D. P., and Coauthors, 2011: The ERA-Interim reanalysis: configuration and
676 performance of the data assimilation system. *Quart. J. Roy. Meteor. Soc.*, **137**, 553–
677 597, <https://doi.org/10.1002/qj.828>.

678

679 Dinku, T., P. Ceccato, E. Grover-Kopec, M. Lemma, S. J. Connor, and C. F.
680 Ropelewski, 2007: Validation of satellite rainfall products over East Africa's complex

681 topography. *Int. J. Remote Sens.*, **28**, 1503–1526,

682 <https://doi.org/10.1080/01431160600954688>.

683

684 Diro, G. T., E. Black, and D. I. F. Grimes, 2008: Seasonal forecasting of Ethiopian

685 spring rains. *Meteor. Appl.*, **15**, 73–83, <https://doi.org/10.1002/met.63>.

686

687 Diro, G. T., D. I. F. Grimes, and E. Black, 2011: Teleconnections between Ethiopian

688 summer rainfall and sea surface temperature: Part II: Seasonal forecasting. *Climate*

689 *Dyn.*, **37**, 121–131, <https://doi.org/10.1007/s00382-010-0896-x>.

690

691 Diro, G. T., A. M. Tompkins, and X. Bi, 2012: Dynamical downscaling of ECMWF

692 Ensemble seasonal forecasts over East Africa with RegCM3. *J. Geophys. Res.*, **117**,

693 D16103, <https://doi.org/10.1029/2011JD016997>.

694

695 Dunning, C. M., E. C. L. Black, and R. P. Allan, 2016: The onset and cessation of

696 seasonal rainfall over Africa. *Geophys. Res.: Atmos.*, **121**, 11405–11424,

697 <https://doi.org/10.1002/2016JD025428>.

698

699 Dutra, E., L. Magnusson, F. Wetterhall, H. L. Cloke, G. Balsamo, S. Bousetta, and

700 F. Pappenberger, 2013: The 2010–2011 drought in the Horn of Africa in ECMWF

701 reanalysis and seasonal forecast products. *Int. J. Climatol.*, **33**, 1720–1729,

702 <https://doi.org/10.1002/joc.3545>.

703

704 FAO, 2018: FAOSTAT Country Indicators. Accessed 27 June 2018,
705 <http://www.fao.org/faostat/en/#country>.
706

707 Funk, C., A. Hoell, S. Shukla, I. Blade, B. Liebmann, J. B. Roberts, F. R. Robertson,
708 and G. Husak, 2014: Predicting East African spring droughts using Pacific and Indian
709 Ocean sea surface temperature indices. *Hydrol. Earth Syst. Sc.*, **18**, 4965–4978,
710 <https://doi.org/10.5194/hess-18-4965-2014>.
711

712 Goddard, L., and M. Dilley, 2005: El Niño: catastrophe or opportunity. *J. Climate*, **18**,
713 651–665, <https://doi.org/10.1175/JCLI-3277.1>.
714

715 Hansen, J. W., S. J. Mason, L. Sun, and A. Tall, 2011: Review of seasonal climate
716 forecasting for agriculture in Sub-Saharan Africa. *Exp. Agr.*, **47**, 205–240,
717 <https://dx.doi.org/10.1017/S0014479710000876>.
718

719 Herrero, M., C. Ringler, J. van de Steeg, P. Thornton, T. Zhu, E. Bryan, A. Omolo, J.
720 Koo, and A. Notenbaert, 2010: Climate variability and climate change and their
721 impacts on Kenya’s agricultural sector. Nairobi, Kenya. ILRI.
722 <https://cgspace.cgiar.org/bitstream/handle/10568/3840/climateVariability.pdf>

723 Hirschi, M., S. I. Seneviratne, V. Alexandrov, F. Boberg, C. Boroneant, O. B.
724 Christensen, H. Formayer, B. Orlowsky, and P. Stepanek, 2011. Observational
725 evidence for soil-moisture impact on hot extremes in southeastern Europe. *Nat.*
726 *Geosci.*, **4**, 17–21, <https://doi.org/10.1038/ngeo1032>
727

728 Kimani, M. W., J. C. B. Hoedjes, and Z. Su, 2017: An Assessment of Satellite-
729 Derived Rainfall Products Relative to Ground Observations over East Africa. *Remote*
730 *Sens.*, **9**, 430, <https://doi.org/10.3390/rs9050430>.
731
732 Kipkogei, O., A. M. Mwanthi, J. B. Mwesigwa, Z. K. K. Atheru, M. A. Wanzala, and G.
733 Artan, 2017: Improved Seasonal Prediction of Rainfall over East Africa for
734 Application in Agriculture: Statistical Downscaling of CFSv2 and GFDL-FLOR. *J.*
735 *Appl. Meteor. Clim.*, **56**, 3229–3243, <https://doi.org/10.1175/JAMC-D-16-0365.1>.
736
737 Kotikot, S. M., and S. M. Onywere, 2015: Application of GIS and remote sensing
738 techniques in frost risk mapping for mitigating agricultural losses in the Aberdare
739 ecosystem, Kenya. *Geocarto International*, **30**, 104–121,
740 <https://doi.org/10.1080/10106049.2014.965758>.
741
742 Lemos, M. C., T. J. Finan, R. W. Fox, D. R. Nelson, and J. Tucker, 2002: The use of
743 seasonal climate forecasting in policymaking: lessons from Northeast Brazil. *Clim.*
744 *Change*, **55**, 479–507, <https://doi.org/10.1023/A:1020785826029>.
745
746 Liebmann, B., M. P. Hoerling, C. Funk, I. Bladé, R. M. Dole, D. Allured, X. Quan, P.
747 Pegion, and J. K. Eischeid, 2014: Understanding recent eastern Horn of Africa
748 rainfall variability and change. *J. Climate*, **27**, 8630–8645,
749 <https://doi.org/10.1175/JCLI-D-13-00714.1>
750

751 MacLachlan, C., and Coauthors, 2014: Global Seasonal forecast system version 5
752 (GloSea5): a high-resolution seasonal forecast system. *Quart. J. Roy. Meteor. Soc.*,
753 **141**, 1072–1084, <https://doi.org/10.1002/qj.2396>.

754

755 MacLeod, D., 2018: Seasonal predictability of onset and cessation of the east
756 African rains. *Wea. Clim. Extremes*, **21**, 27–35,
757 <https://doi.org/10.1016/j.wace.2018.05.003>.

758

759 Murphy, A. H., and E. S. Epstein, 1989: Skill scores and correlation coefficients in
760 model verification. *Mon. Wea. Rev.*, **117**, 572–582, [https://doi.org/10.1175/1520-
761 0493\(1989\)117%3C0572:SSACCI%3E2.0.CO;2](https://doi.org/10.1175/1520-0493(1989)117%3C0572:SSACCI%3E2.0.CO;2).

762

763 Mutai, C. C., and M. N. Ward, 2000: East African rainfall and the tropical
764 circulation/convection on intraseasonal to interannual timescales. *J. Climate.*, **13**,
765 3915–3939, [https://doi.org/10.1175/1520-
766 0442\(2000\)013%3C3915:EARATT%3E2.0.CO;2](https://doi.org/10.1175/1520-0442(2000)013%3C3915:EARATT%3E2.0.CO;2)

767

768 Mwangi, E., F. Wetterhall, E. Dutra, F. Di Giuseppe, and F. Pappenberger, 2014:
769 Forecasting droughts in East Africa. *Hydrol. Earth Syst. Sc.*, **18**, 611–620,
770 <https://doi.org/10.5194/hess-18-611-2014>, 2014.

771

772 Nicholson, S. E., 2014: The Predictability of Rainfall over the Greater Horn of Africa.
773 Part I: Prediction of Seasonal Rainfall. *J. Hydrometeorol.*, **15**, 1011–1027,
774 <https://doi.org/10.1175/JHM-D-13-062.1>.

775

776 Nicholson, S. E., 2015: The predictability of rainfall over the Greater Horn of Africa.
777 Part II: Prediction of monthly rainfall during the long rains. *J. Hydrometeorol.*, **16**,
778 2001–2012, <https://doi.org/10.1175/JHM-D-14-0138.1>.

779

780 Nicholson, S. E., 2017: Climate and climatic variability of rainfall over eastern Africa.
781 *Rev. Geophys.*, **55**, 590–635, <https://doi.org/10.1002/2016RG000544>.

782

783 Nicholson, S. E., and J. Kim, 1997: The relationship of the El Niño–southern
784 oscillation to African rainfall. *Int. J. Climatol.*, **17**, 117–135,
785 [https://doi.org/10.1002/\(SICI\)1097-0088\(199702\)17:2%3C117::AID-](https://doi.org/10.1002/(SICI)1097-0088(199702)17:2%3C117::AID-JOC84%3E3.0.CO;2-O)
786 [JOC84%3E3.0.CO;2-O](https://doi.org/10.1002/(SICI)1097-0088(199702)17:2%3C117::AID-JOC84%3E3.0.CO;2-O).

787

788 Patt, A., and C. Gwata, 2002: Effective seasonal climate forecast applications:
789 examining constraints for subsistence farmers in Zimbabwe. *Global Environ.*
790 *Change*, **12**, 185–195, [https://doi.org/10.1016/S0959-3780\(02\)00013-4](https://doi.org/10.1016/S0959-3780(02)00013-4).

791

792 Ropelewski, C. F., and M. S. Halpert, 1987: Global and regional scale precipitation
793 patterns associated with the El Niño/Southern Oscillation. *Mon. Wea. Rev.*, **115**,
794 1606–1626, [https://doi.org/10.1175/1520-](https://doi.org/10.1175/1520-0493(1987)115%3C1606:GARSPP%3E2.0.CO;2)
795 [0493\(1987\)115%3C1606:GARSPP%3E2.0.CO;2](https://doi.org/10.1175/1520-0493(1987)115%3C1606:GARSPP%3E2.0.CO;2).

796 Russo, S., A. F. Marchese, J. Sillmann, and G. Immé, 2016. When will unusual heat
797 waves become normal in a warming Africa? *Environ. Res. Lett.*, **11**, 054016,
798 <http://dx.doi.org/10.1088/1748-9326/11/5/054016>

799

800 Saha, S., and Coauthors, 2014: The NCEP Climate Forecast System Version 2. *J.*
801 *Climate*, **27**, 2185–2208, <https://doi.org/10.1175/JCLI-D-12-00823.1>.

802

803 Saji, N. H., B. N. Goswami, P. N. Vinayachandran, and T. Yamagata, 1999: A dipole
804 mode in the tropical Indian Ocean. *Nature*, **401**, 360–363,
805 <https://doi.org/10.1038/43854>.

806

807 Trenberth, K. E., 1997: The Definition of El Niño. *B. Am. Meteorol. Soc.*, **78**, 2771–
808 2777, [https://doi.org/10.1175/1520-](https://doi.org/10.1175/1520-0477(1997)078%3C2771:TDOENO%3E2.0.CO;2)
809 [0477\(1997\)078%3C2771:TDOENO%3E2.0.CO;2](https://doi.org/10.1175/1520-0477(1997)078%3C2771:TDOENO%3E2.0.CO;2).

810

811 van den Hurk, B., F. Doblas-Reyes, G. Balsamo, R. D. Koster, S. I. Seneviratne, and
812 H. Camargo, 2012: Soil moisture effects on seasonal temperature and precipitation
813 forecast scores in Europe. *Clim. Dyn.*, **38**, 349–362, [https://doi.org/10.1007/s00382-](https://doi.org/10.1007/s00382-010-0956-2)
814 [010-0956-2](https://doi.org/10.1007/s00382-010-0956-2).

815

816 Vellinga, M., and S. F. Milton, 2018: Drivers of interannual variability of the East
817 African “Long Rains”. *Q. J. Roy. Meteor Soc.*, **144**, 861–876.
818 <https://doi.org/10.1002/qj.3263>

819

820 Vitart, F., A. W. Robertson, and D. L. Anderson, 2012: Subseasonal to Seasonal
821 Prediction Project: Bridging the gap between weather and climate. *B. World Meteor.*
822 *Org.*, **61**, 23–28.

823

824 Walker, D. P., C. E. Birch, J. H. Marsham, A. A. Scaife, R. J. Graham, and Z. T.
825 Segele, 2019: Skill of dynamical and GHACOF consensus seasonal forecasts of
826 East African rainfall. *Climate Dyn.*, <https://doi.org/10.1007/s00382-019-04835-9>.

827

828 Webster, P. J., and S. Yang, 1992: Monsoon and ENSO: Selectively interactive
829 systems. *Quart. J. Roy. Meteor. Soc.*, **118**, 825–877,
830 <https://doi.org/10.1002/qj.49711850705>.

831

832 Weisheimer, A., and T. N. Palmer, 2014: On the reliability of seasonal climate
833 forecasts. *J. Roy. Soc. Interface*, **11**, 20131162,
834 <https://doi.org/10.1098/rsif.2013.1162>.

835

836

837

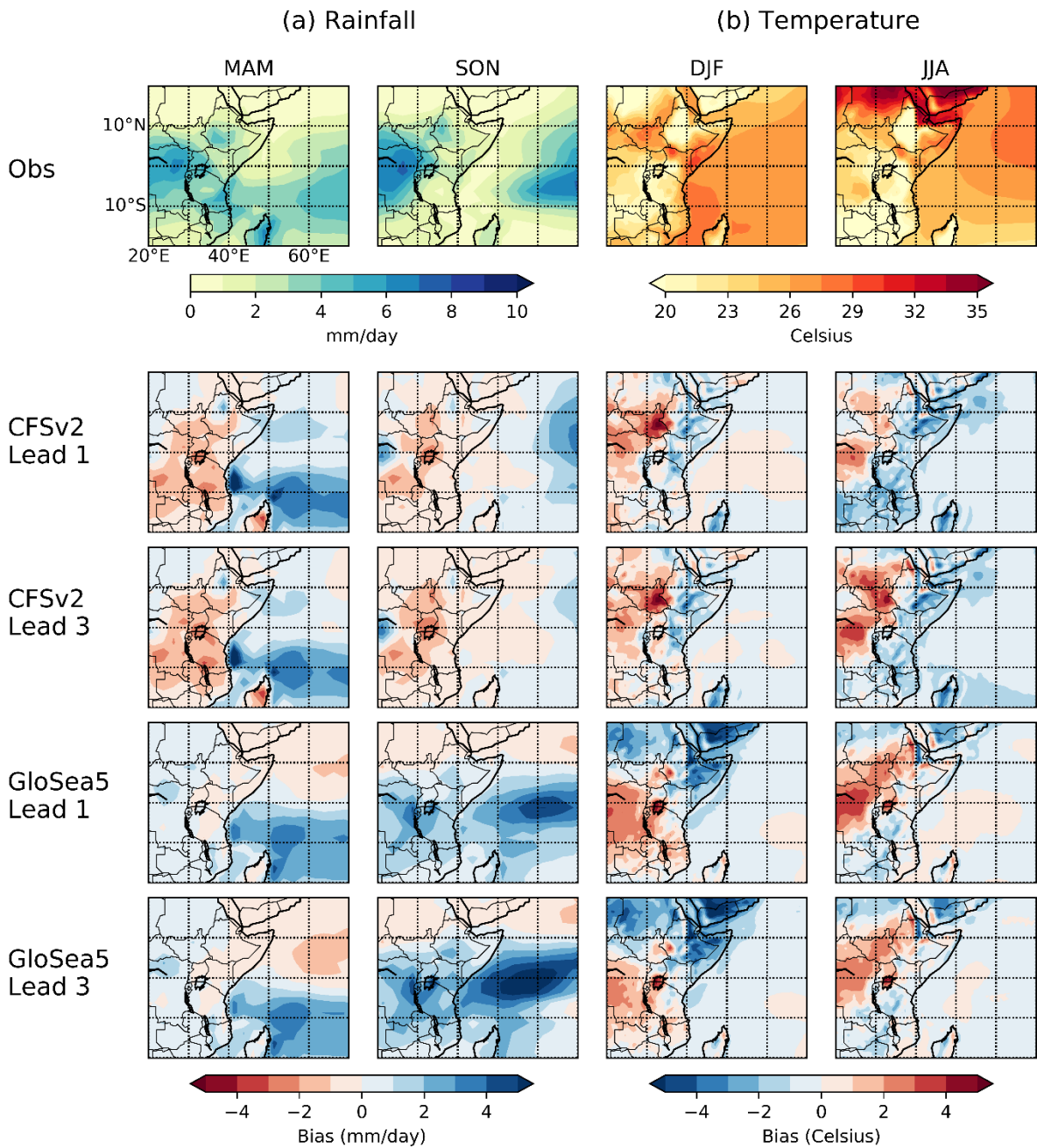
838

839

840

841

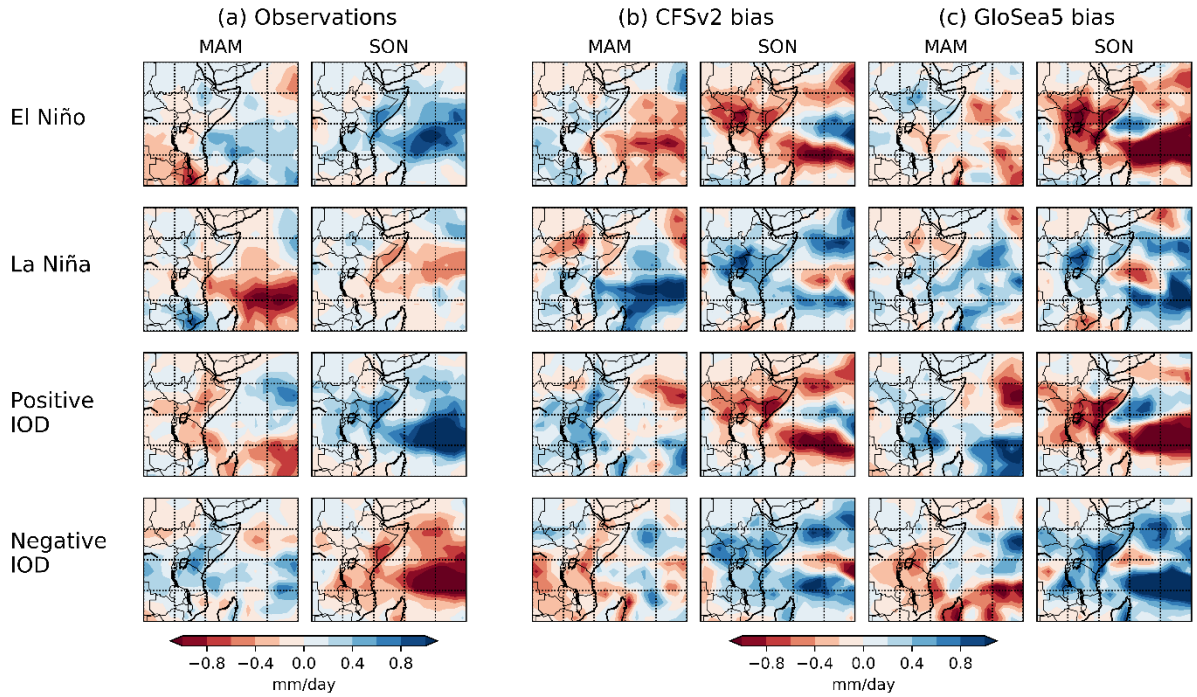
842



843

844

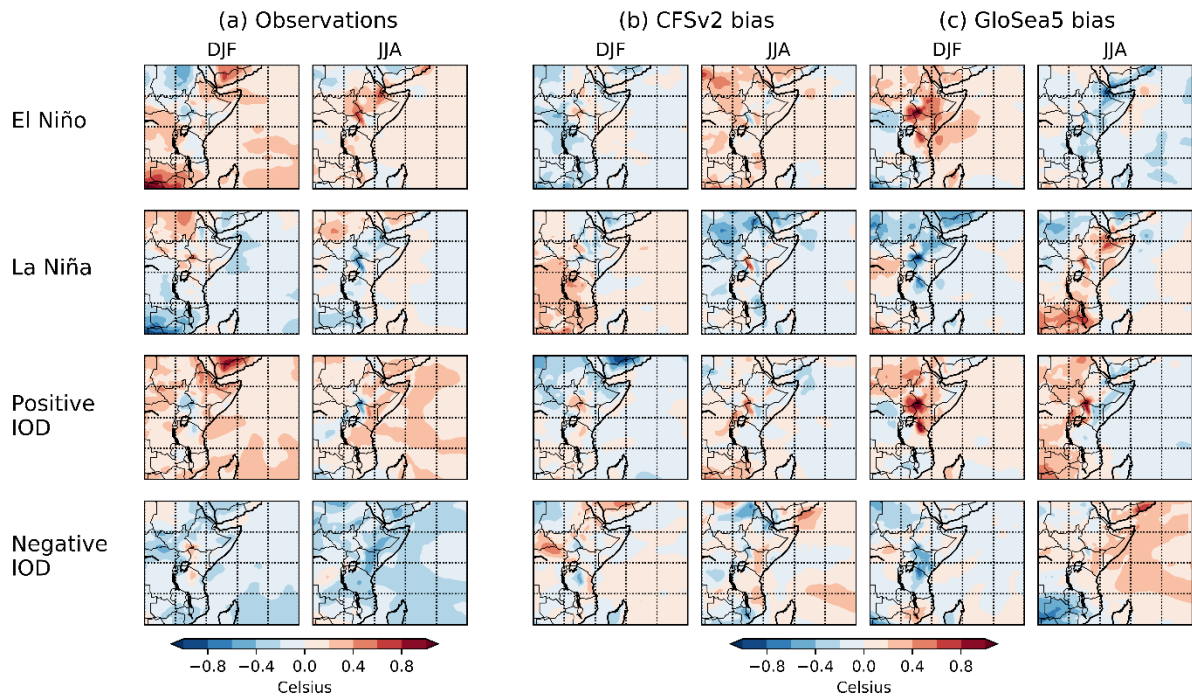
845 Figure 1. Seasonal mean observations and model biases for (a) rainfall (mm day^{-1}) in
 846 MAM and SON (b) 2m air temperature ($^{\circ}\text{C}$) in DJF and JJA. Observational data are
 847 for the period 1982-2015 from (a) GPCP and (b) ERA-Interim; model biases are for
 848 their own time periods, lead times are in months ahead of the season.



850

851 Figure 2. Anomalies in observations during ENSO and IOD phases for rainfall (mm
 852 day⁻¹) in MAM and SON, and model biases in those phases relative to the model
 853 mean bias at one month lead time. These are composites based on years in which
 854 observed SSTs fall into tercile categories (11 or 12 years for observations, 10 years
 855 for CFSv2, 8 years for GloSea5).

856



857

858

Figure 3. Anomalies in observations during ENSO and IOD phases for 2m air

859

temperature ($^{\circ}\text{C}$) in DJF and JJA, and model biases in those phases relative to the

860

model mean bias at one month lead time. These are composites based on years in

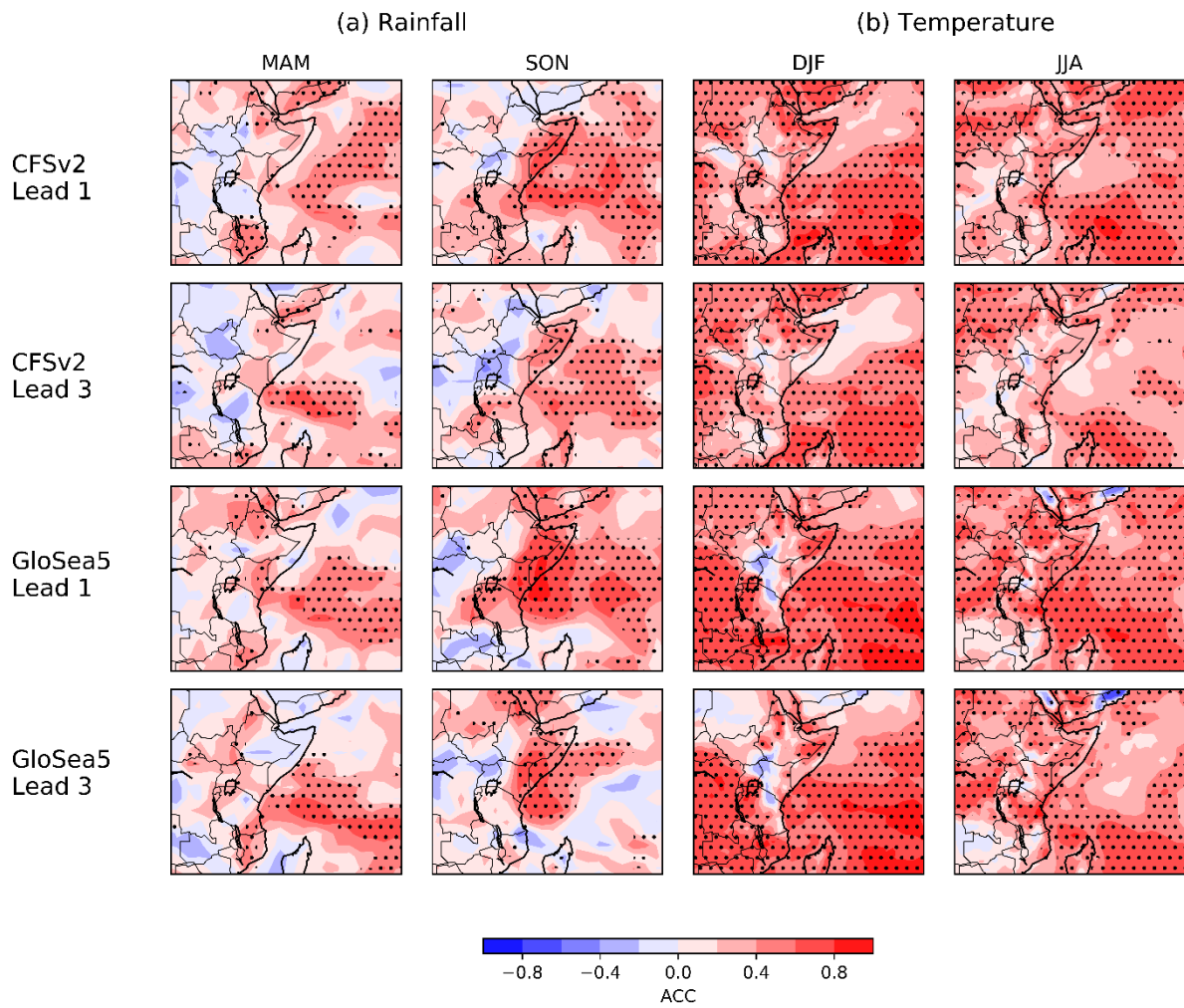
861

which observed SSTs fall into tercile categories (11 or 12 years for observations, 10

862

years for CFSv2, 8 years for GloSea5).

863



864

865 Figure 4. Temporal Anomaly Correlation Coefficients of re-forecasts of (a) rainfall in
 866 MAM and SON and (b) 2m air temperature in DJF and JJA. Lead times are in
 867 months ahead of the season. Stippling corresponds to areas where the correlation is
 868 significant ($p \leq 0.05$).

869

870

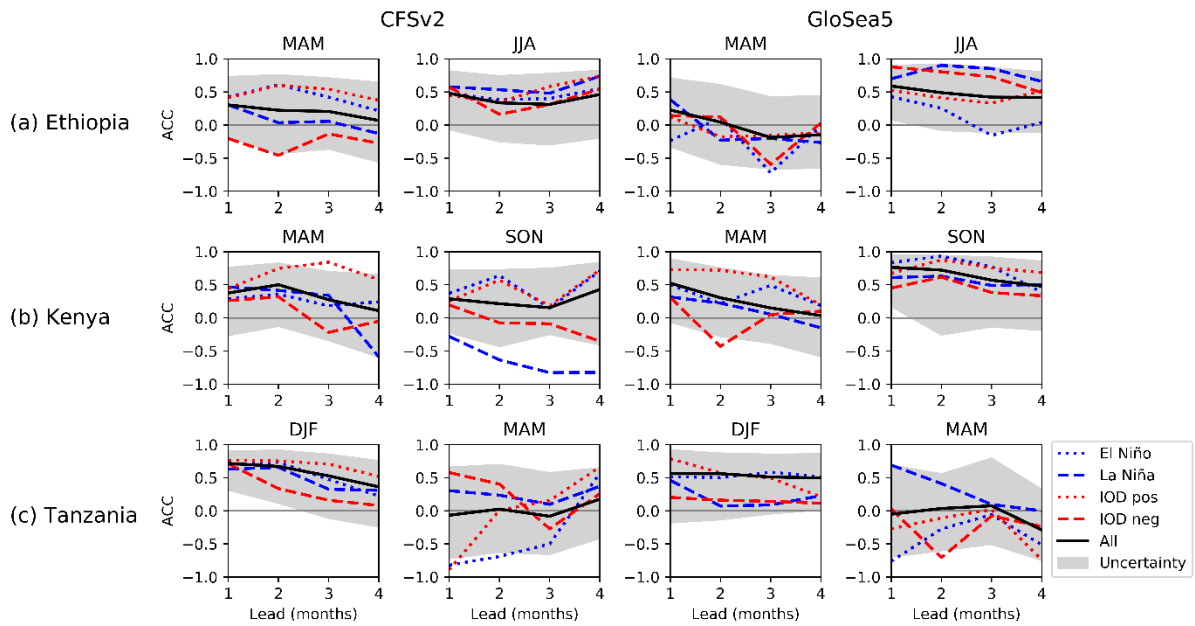
871

872

873

874

875

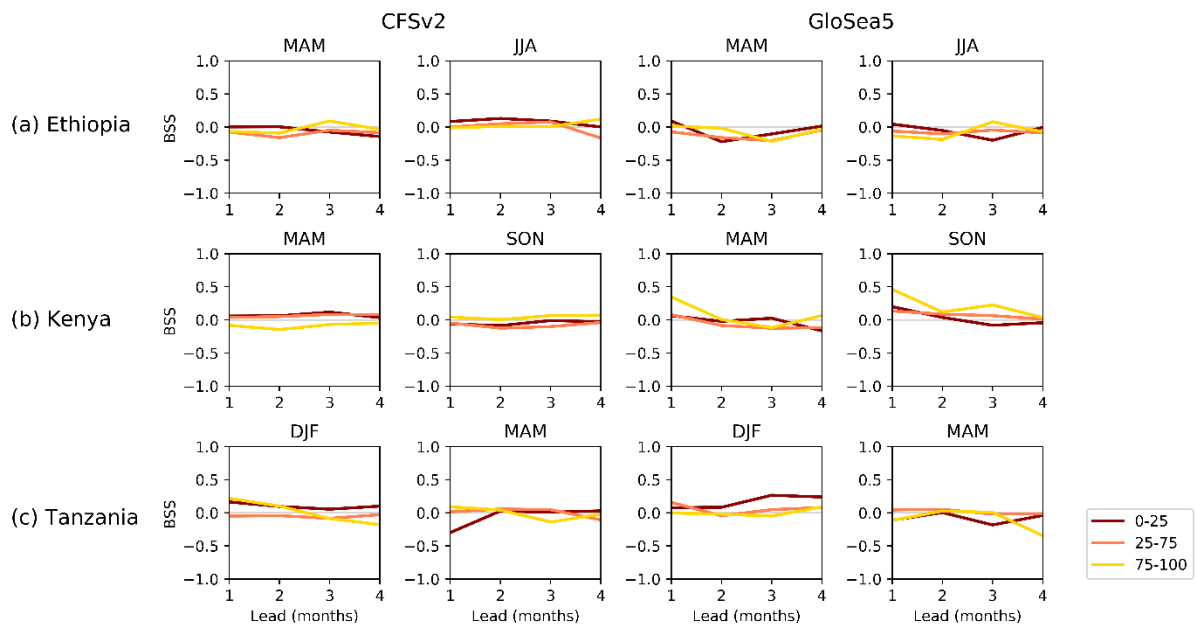


876

877

878 Figure 5. Country-average scale temporal Anomaly Correlation Coefficients (ACCs)
879 of rainfall re-forecasts from (left) CFSv2 and (right) GloSea5 for key rainy seasons in
880 (a) Ethiopia, (b) Kenya and (c) Tanzania. ACCs are shown for all years (black) and
881 years in ENSO and IOD phases (colours); the uncertainty (grey) represents the 5th-
882 95th percentiles from bootstrapping with the number of years in the ENSO and IOD
883 phases.

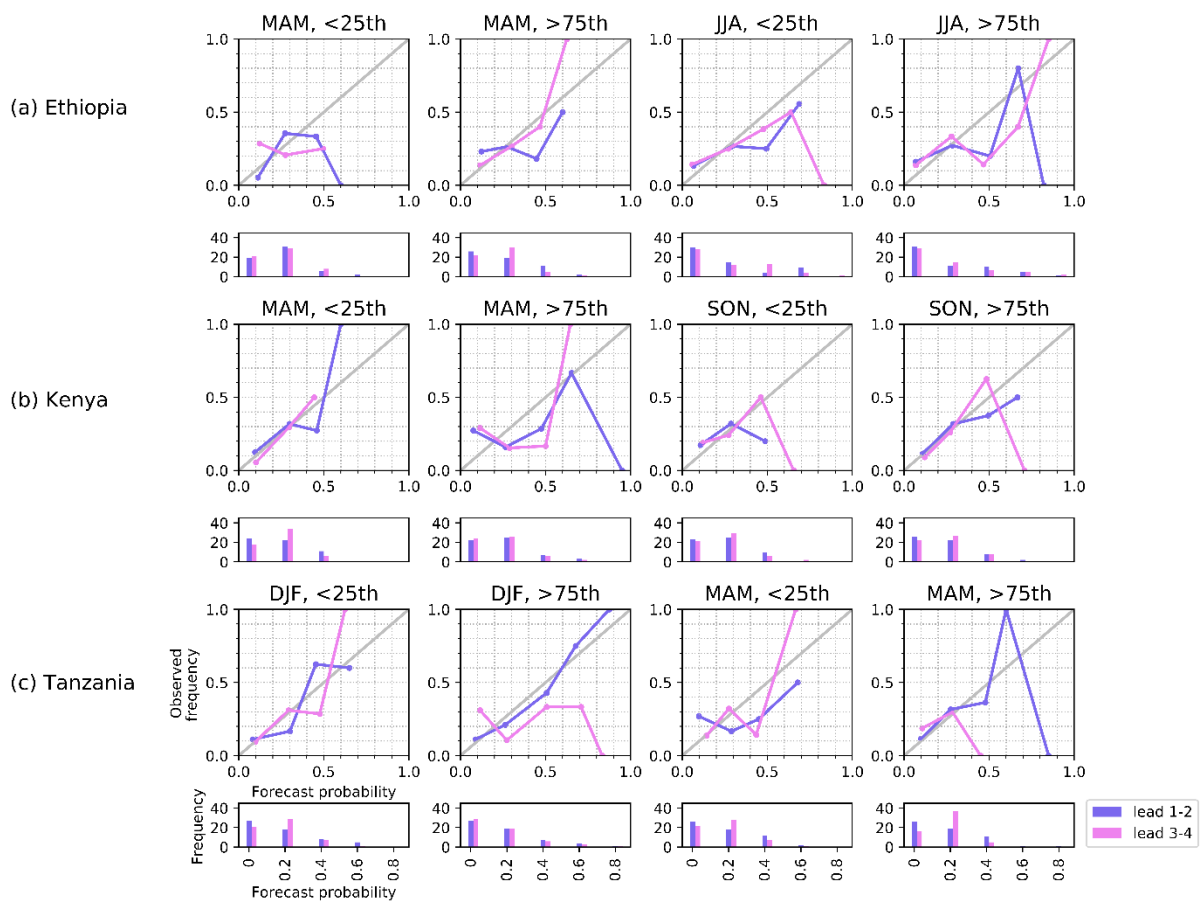
884



885

886 Figure 6. Country-average scale Brier Skill Scores for rainfall re-forecasts using
 887 percentiles based on model re-forecast climatologies to define events, from (left)
 888 CFSv2 and (right) GloSea5 for key rainy seasons in (a) Ethiopia, (b) Kenya and (c).
 889 Colours represent dry (red), normal (orange) and wet (yellow) events.

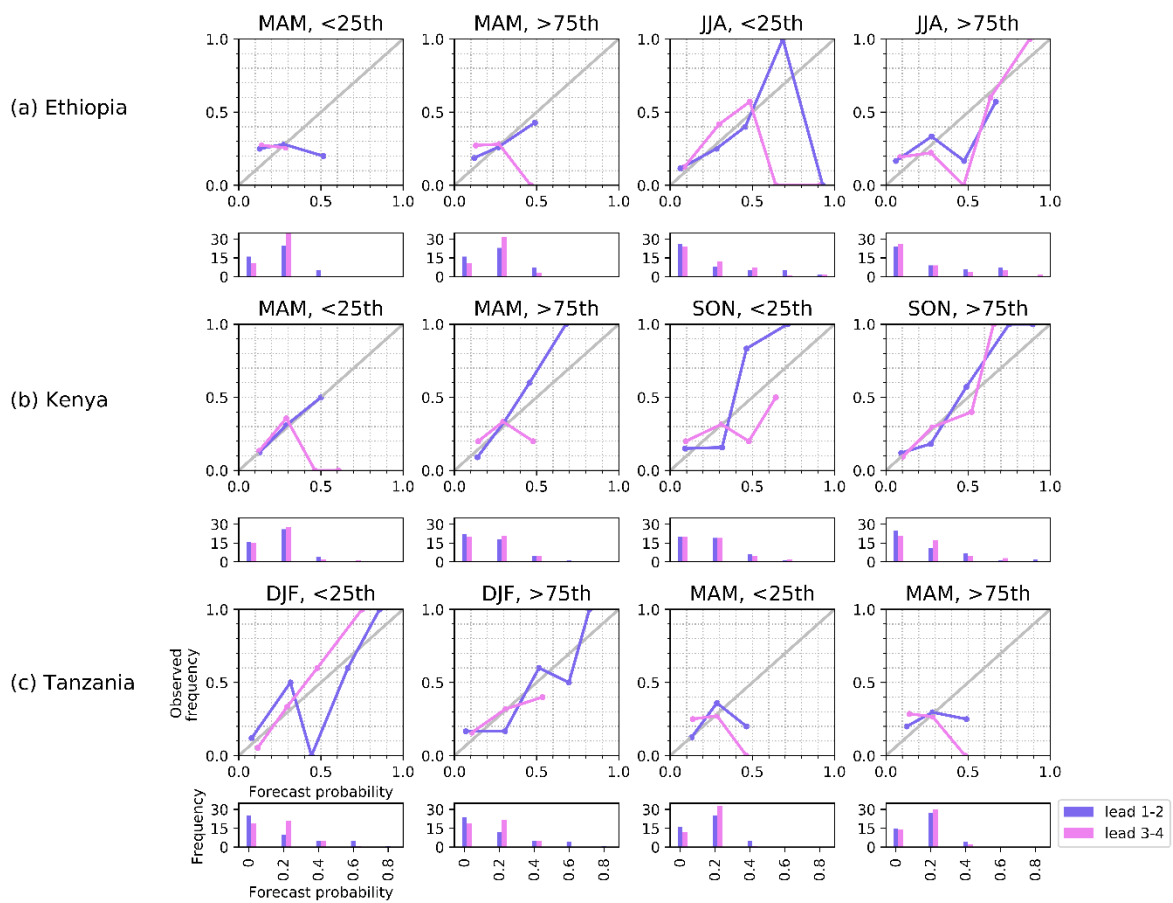
890



891

892 Figure 7. Country-average scale reliability diagrams for rainfall re-forecasts from
 893 CFSv2 using percentiles based on model re-forecast climatologies to define events
 894 below the 25th and above the 75th percentiles, for key rainy seasons in (a) Ethiopia,
 895 (b) Kenya and (c) Tanzania. Colours represent reliability for lead 1-2 (purple) and
 896 lead 3-4 (pink) and the 1:1 line (grey).

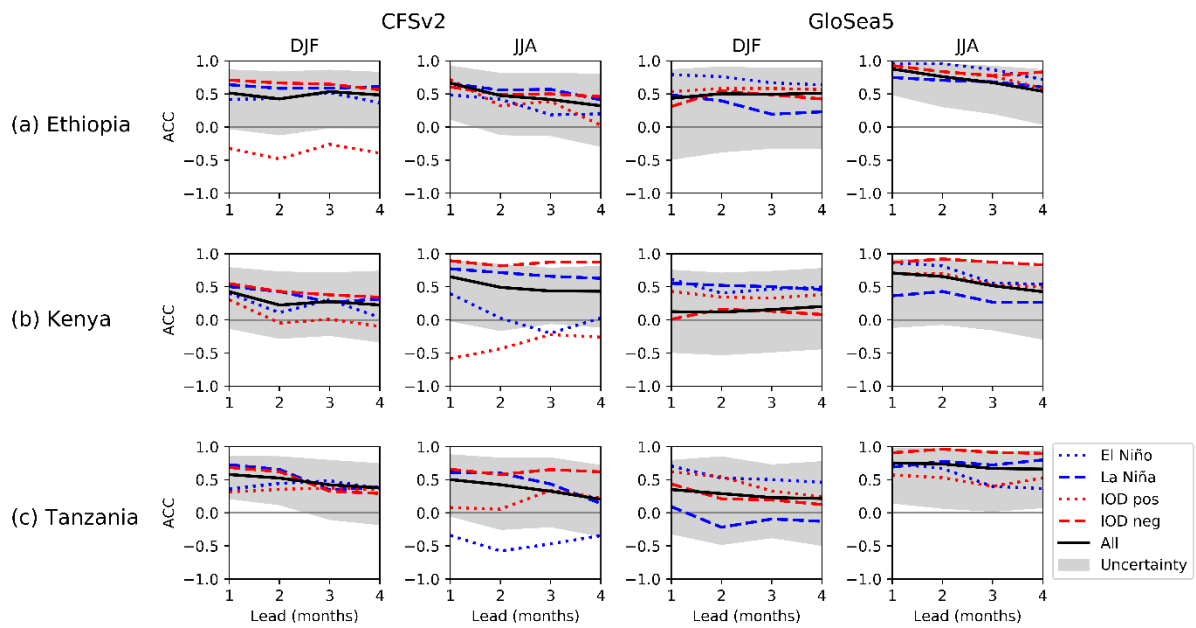
897



898

899 Figure 8. Country-average scale reliability diagrams for rainfall re-forecasts from
 900 GloSea5 using percentiles based on model re-forecast climatologies to define events
 901 below the 25th and above the 75th percentiles, for key rainy seasons in (a) Ethiopia,
 902 (b) Kenya and (c) Tanzania. Colours represent reliability for lead 1-2 (purple) and
 903 lead 3-4 (pink) and the 1:1 line (grey).

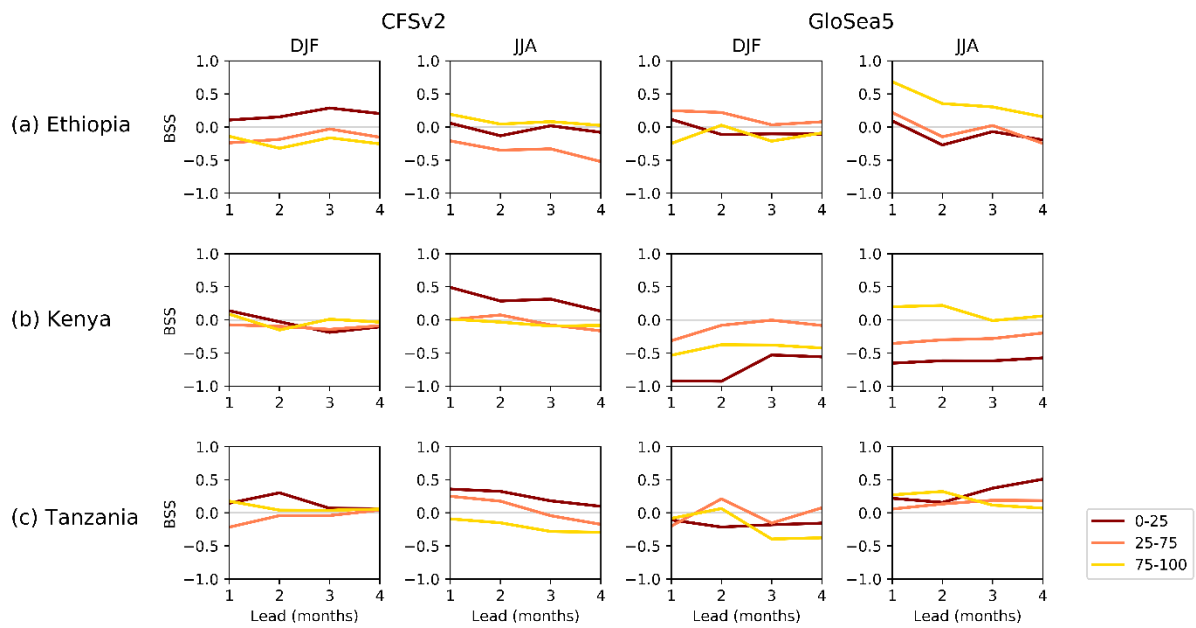
904



905

906 Figure 9. Country-average scale temporal Anomaly Correlation Coefficients (ACCs)
 907 of 2m air temperature re-forecasts from (left) CFSv2 and (right) GloSea5 for DJF and
 908 JJA in (a) Ethiopia, (b) Kenya and (c) Tanzania. ACCs are shown for all years (black)
 909 and years in ENSO and IOD phases (colours); the uncertainty (grey) represents the
 910 5th-95th percentiles from bootstrapping with the number of years in the ENSO and
 911 IOD phases.

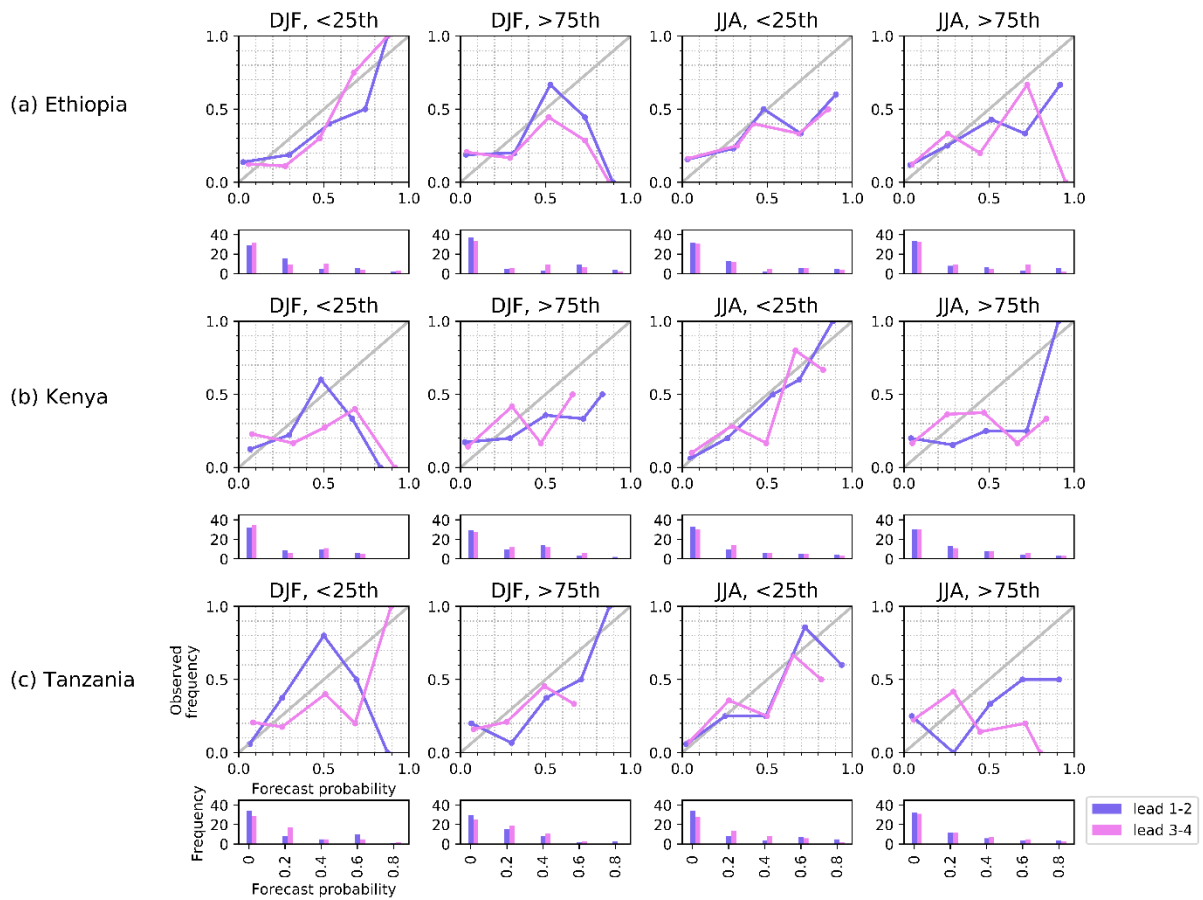
912



913

914 Figure 10. Country-average scale Brier Skill Scores for 2m air temperature re-
 915 forecasts using percentiles based on model re-forecast climatologies to define
 916 events, from (left) CFSv2 and (right) GloSea5 for DJF and JJA in (a) Ethiopia, (b)
 917 Kenya and (c) Tanzania. Colours represent cool (red), normal (orange) and warm
 918 (yellow) events.

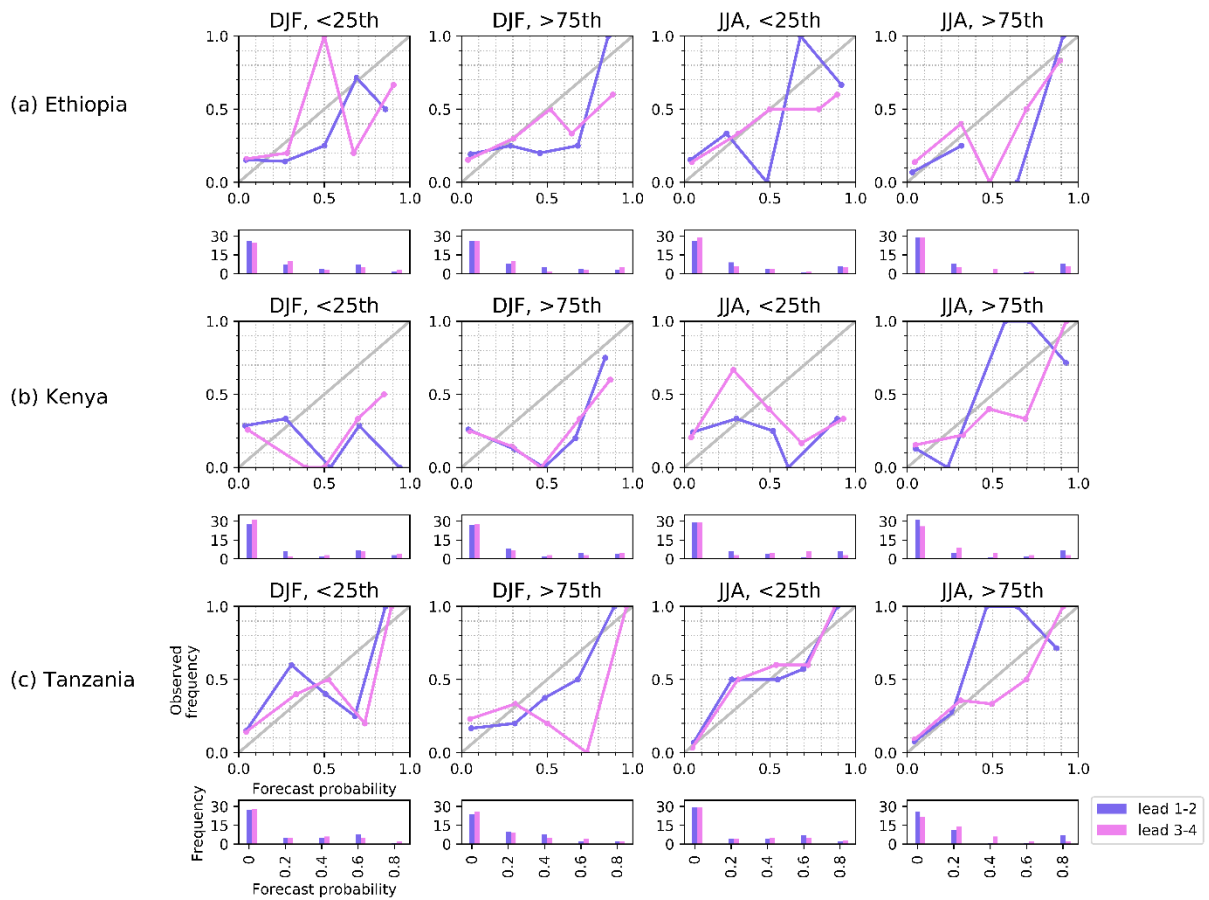
919



920

921 Figure 11. Country-average scale reliability diagrams for 2m air temperature re-
 922 forecasts from CFSv2 using percentiles based on model re-forecast climatologies to
 923 define events below the 25th and above the 75th percentiles, for DJF and JJA in (a)
 924 Ethiopia, (b) Kenya and (c) Tanzania. Colours represent reliability for lead 1-2
 925 (purple) and lead 3-4 (pink) and the 1:1 line (grey).

926



927

928 Figure 12. Country-average scale reliability diagrams for 2m air temperature re-
 929 forecasts from GloSea5 using percentiles based on model re-forecast climatologies
 930 to define events below the 25th and above the 75th percentiles, for DJF and JJA in (a)
 931 Ethiopia, (b) Kenya and (c) Tanzania. Colours represent reliability for lead 1-2
 932 (purple) and lead 3-4 (pink) and the 1:1 line (grey).

933

934

935

936

937

938

		Rainfall															
		ACC				BSS 0-25				BSS 25-75				BSS 75-100			
		CFSv2 Lead 1	CFSv2 Lead 2	GloSea5 Lead 1	GloSea5 Lead 2	CFSv2 Lead 1	CFSv2 Lead 2	GloSea5 Lead 1	GloSea5 Lead 2	CFSv2 Lead 1	CFSv2 Lead 2	GloSea5 Lead 1	GloSea5 Lead 2	CFSv2 Lead 1	CFSv2 Lead 2	GloSea5 Lead 1	GloSea5 Lead 2
Ethiopia	MAM	0.30	0.22	0.23	0.04	0.00	0.00	0.09	-0.22	-0.08	-0.16	-0.07	-0.16	-0.07	-0.09	0.02	-0.02
	JJA	0.48	0.33	0.59	0.49	0.08	0.13	0.04	-0.05	0.00	0.05	-0.06	-0.10	-0.01	0.01	-0.13	-0.19
Kenya	MAM	0.38	0.50	0.53	0.30	0.06	0.06	0.06	-0.02	0.04	0.05	0.08	-0.08	-0.08	-0.15	0.35	0.01
	SON	0.29	0.21	0.76	0.72	-0.06	-0.09	0.20	0.04	-0.05	-0.12	0.13	0.09	0.04	0.01	0.46	0.12
Tanzania	DJF	0.72	0.67	0.56	0.56	0.16	0.10	0.08	0.08	-0.05	-0.04	0.16	-0.04	0.22	0.10	0.02	-0.02
	MAM	-0.07	0.03	-0.05	0.04	-0.30	0.03	-0.11	0.00	0.01	0.06	0.04	0.05	0.09	0.04	-0.13	-0.19

939

940 Table 1. Summary of ACC and BSS country results for rainfall forecasts at lead 1 and lead 2. Values are shown to 2 decimal
941 places, with bold signifying ACC values that are significant ($p \leq 0.05$) and BSS values where the 5th-95th percentile uncertainty range
942 from bootstrapping lies above 0.0.

943

944

945

946

947

948

949

		Temperature															
		ACC				BSS 0-25				BSS 25-75				BSS 75-100			
		CFSv2 Lead 1	CFSv2 Lead 2	GloSea5 Lead 1	GloSea5 Lead 2	CFSv2 Lead 1	CFSv2 Lead 2	GloSea5 Lead 1	GloSea5 Lead 2	CFSv2 Lead 1	CFSv2 Lead 2	GloSea5 Lead 1	GloSea5 Lead 2	CFSv2 Lead 1	CFSv2 Lead 2	GloSea5 Lead 1	GloSea5 Lead 2
Ethiopia	DJF	0.51	0.42	0.43	0.50	0.11	0.15	0.11	-0.11	-0.24	-0.19	0.25	0.22	-0.14	-0.32	-0.25	0.03
	JJA	0.66	0.47	0.88	0.76	0.06	-0.13	0.09	-0.27	-0.21	-0.35	0.22	-0.15	0.19	0.04	0.68	0.35
Kenya	DJF	0.43	0.22	0.12	0.12	0.14	-0.03	-0.92	-0.93	-0.07	-0.10	-0.31	-0.08	0.09	-0.15	-0.53	-0.37
	JJA	0.65	0.49	0.71	0.66	0.49	0.29	-0.65	-0.62	0.00	0.07	-0.36	-0.30	0.01	-0.03	0.20	0.22
Tanzania	DJF	0.58	0.52	0.35	0.29	0.15	0.30	-0.12	-0.22	-0.22	-0.04	-0.20	0.21	0.18	0.04	-0.09	0.06
	JJA	0.50	0.42	0.75	0.74	0.36	0.32	0.22	0.16	0.25	0.18	0.06	0.13	-0.09	-0.15	0.27	0.32

950

951 Table 2. Summary of ACC and BSS country results for temperature forecasts at lead 1 and lead 2. Values are shown to 2 decimal
 952 places, with bold signifying ACC values that are significant ($p \leq 0.05$) and BSS values where the 5th-95th percentile uncertainty range
 953 from bootstrapping lies above 0.0.

954